AGU100 ADVANCING EARTH AND SPACE SCIENCE

JGR

Journal of Geophysical Research: Solid Earth

RESEARCH ARTICLE

10.1029/2018JB016438

Key Points:
- We introduce stress-based tomography as a method to characterize the fracture network and its heterogeneity in deep geothermal reservoirs
- Stress heterogeneities at borehole scale are applied to calibrate DFN realizations
- The methodology is successfully tested to image simple synthetic and outcrop-based fracture networks

Supporting Information:
- Supporting Information S1
- Data Set S1

Correspondence to:
M. J. Afshari Moein,
mohammad.moein@erdw.ethz.ch

Citation:
Afshari Moein, M. J., Somogyvári, M., Valley, B., Jalali, M., Loew, S., & Bayer, P. (2018). Fracture network characterization using stress-based tomography. *Journal of Geophysical Research: Solid Earth*, *123*, 9324–9340. https://doi.org/10.1029/2018JB016438

Received 30 JUL 2018
Accepted 23 OCT 2018
Accepted article online 29 OCT 2018
Published online 28 NOV 2018

Fracture Network Characterization Using Stress-Based Tomography

Mohammad Javad Afshari Moein[1], Márk Somogyvári[2], Benoît Valley[3], Mohammadreza Jalali[1], Simon Loew[1], and Peter Bayer[4]

[1]Department of Earth Sciences, Geological Institute, ETH Zürich, Zurich, Switzerland, [2]Institute of Mathematics, University of Potsdam, Potsdam, Germany, [3]Center for Hydrogeology and Geothermics, University of Neuchâtel, Neuchâtel, Switzerland, [4]Institute of new Energy Systems, Ingolstadt University of Applied Sciences, Ingolstadt, Germany

Abstract Information on structural features of a fracture network at early stages of Enhanced Geothermal System development is mostly restricted to borehole images and, if available, outcrop data. However, using this information to image discontinuities in deep reservoirs is difficult. Wellbore failure data provides only some information on components of the in situ stress state and its heterogeneity. Our working hypothesis is that slip on natural fractures primarily controls these stress heterogeneities. Based on this, we introduce stress-based tomography in a Bayesian framework to characterize the fracture network and its heterogeneity in potential Enhanced Geothermal System reservoirs. In this procedure, first a random initial discrete fracture network (DFN) realization is generated based on prior information about the network. The observations needed to calibrate the DFN are based on local variations of the orientation and magnitude of at least one principal stress component along boreholes. A Markov Chain Monte Carlo sequence is employed to update the DFN iteratively by a fracture translation within the domain. The Markov sequence compares the simulated stress profile with the observed stress profiles in the borehole, evaluates each iteration with Metropolis-Hastings acceptance criteria, and stores acceptable DFN realizations in an ensemble. Finally, this obtained ensemble is used to visualize the potential occurrence of fractures in a probability map, indicating possible fracture locations and lengths. We test this methodology to reconstruct simple synthetic and more complex outcrop-based fracture networks and successfully image the significant fractures in the domain.

1. Introduction

Although the amount of thermal energy in the Earth's crust is enormous and could substantially contribute to the world's energy supply (Tester et al., 2006), the current geothermal energy production is limited to particular geological locations where water is circulated at sufficient flow rates through hot rock masses. In a standard geological setting, the minimum temperatures, (>120 °C) for producing electricity from geothermal fluids, are mostly found in crystalline basements between 4- and 6-km depth (Evans, 2015), where the permeability is typically low (Achtziger-Zupančič et al., 2017). These systems, usually known as Enhanced Geothermal Systems (EGS), require hydraulic stimulation (i.e., massive fluid injections) to increase the natural flow rates. Permeability creation is expected to improve the heat exchange capacity and thus permit sustainable heat extraction. Flow in EGS develops primarily in the fracture network (Davatzes & Hickman, 2010; Genter et al., 2010) and injecting high-pressure fluid reduces the effective stress on fracture planes, which results in rock mass deformation due to poroelastic interactions. Since these systems are for the most part critically stressed (i.e., close to failure), fluid injections may induce slip on preexisting discontinuity planes (Evans, 2005). However, the mechanisms of permeability enhancement in hydraulic stimulation are not entirely understood (Amann et al., 2017; Evans, Genter, & Sausse, 2005). Such failures are mostly associated with seismic activity that represents a common problem in EGS developments (Davies et al., 2013; Ellsworth, 2013; Evans et al., 2012; Giardini, 2009). For example, high level of seismic activity led to the suspension of Basel, 2006, and Saint-Gallen, 2013, geothermal projects in Switzerland (Edwards et al., 2015; Häring et al., 2008; Moeck et al., 2015). Hydraulic stimulation scenarios should increase the permeability while keeping the seismicity on a safe and nondamaging level (Evans, 2015). Induced seismicity is a complex interaction between the natural fractures and in situ stress change caused by fluid pressure (Evans, Moriya, et al., 2005; Gaucher et al., 2015).

A geological model with a reliable representation of lithological domains and characterization of the fracture network is key to the design of reservoir creation strategies. Furthermore, it is fundamental to quantitatively

analyze the possible relations among the spatial, temporal, or magnitude distribution of induced seismicity and thermo-hydraulic-mechanical characteristics of a fractured rock mass, which is not yet fully understood (Amann et al., 2017). Such a geological model is also crucial for real-time monitoring and seismic risk assessments of a hydraulic stimulation. A geological model requires a complete reservoir characterization, with information on important fracture attributes like density, orientation, type, aperture, and length distributions.

The primary information on the natural fractures in deep reservoirs stems from borehole image logs (e.g., optical televiewer or ultrasonic logs). These images provide limited information on the location and orientation of fractures if they cut through the borehole. Statistical analysis of fractures on boreholes or analogs permits the definition of fracture sets (Ziegler et al., 2015) and also provides the spacing distribution within each fracture set (Moein et al., 2016). However, a deterministic reconstruction of three-dimensional (3-D) fracture networks from even a few boreholes is difficult. Borehole data capture local deterministic elements of a fracture network. However, other items in the surrounding network can only be approximated or described in a probabilistic way (e.g., Illman et al., 2009; Karra et al., 2018; Tezuka & Watanabe, 2000). Thus, stochastic realizations often referred as discrete fracture networks (DFN) are generated based on a statistical characterization of fracture network attributes (e.g., Afshari Moein, 2018; Berrone et al., 2017; Dreuzy et al., 2012).

One possible approach is to limit the 3-D spatial distribution of fractures using stereological relationships, as proposed by Darcel, Bour and Davy (2003). However, the application of these relationships to borehole data still includes a significant uncertainty, even if the fracture length distribution is known (Afshari Moein et al., 2018). Induced microseismicity is another source of information that may reflect some geometrical aspects of fracture network (Afshari Moein et al., 2018; Evans, Moriya, et al., 2005; Moriya et al., 2003; Williams-Stroud et al., 2010). However, this information becomes available only after the execution of hydraulic stimulation and thus is not available in time for stimulation design purposes.

A fundamental point for our work is that natural forces largely influence the in situ stress state in geological settings (e.g., Barton & Zoback, 1994; McNamara et al., 2015; Pierdominici et al., 2011; Rajabi et al., 2017; Sahara et al., 2014; Valley, 2007; Yale, 2003). Stress fluctuations on boreholes often show strong heterogeneities (e.g., Schoenball & Davatzes, 2017; Shamir & Zoback, 1992; Valley & Evans, 2007) that may also be characterized by scaling relationships (e.g., Blake & Davatzes, 2011; Day-Lewis et al., 2010; Valley & Evans, 2014). These observations also suggest that the characteristics of the fracture network affect the stress variability within the rock mass. If only a single fracture is present in the rock mass, the size of stress perturbation depends primarily on the size of the fracture (Pollard & Segall, 1987). Nevertheless, in the situation where multiple fractures interact, the relation between the in situ stress fluctuations and critical characteristics of a fracture network is complex and not completely understood (Rutqvist, 2015; Tsang et al., 2018; Valley et al., 2014).

In the present study, we propose constraining the critical characteristics of the fracture network using in situ stress heterogeneities inferred from borehole images. Valley et al. (2014) suggested an inversion approach to extract the geometrical characteristics of a fracture network by minimizing the difference between computed and observed horizontal stress orientation variability in a single borehole. This approach successfully reconstructed the geometry of a single fracture intersecting the borehole. On the other hand, the plan failed to determine the geometry of complex fracture networks, in which all of the fractures do not necessarily intersect the borehole. The inversion technique that we present, also referred to as stress-based tomography, reconstructs the fracture network geometry using the vertical stress profiles through a Bayesian approach. We apply a quasi-static geomechanical simulator to model the stress variability within a fracture network efficiently and to extract the associated borehole stress profiles. During the inversion process, we also use prior knowledge on mechanical properties of the rock mass and the statistical properties of fracture attributes (length, orientation and density). The inversion delivers a probability map that illuminates the probable fracture locations and their lengths. We test this approach through the use of a simple synthetic DFN, and a more complex outcrop mapped DFN. Finally, we discuss the applications and limitations of the inversion technique for deep boreholes and present an outlook for future developments.

2. In Situ Stress Characterization

Information on the in situ stress state is fundamental to any seismo-thermo-hydro-mechanical characterization of fractured reservoirs (Amann et al., 2017; Ghassemi, 2012; Preisig et al., 2015; Zoback, 2010). Complete characterization of a stress tensor requires six parameters at any point. The assumption that one principal

stress, S_v, is vertical and equal to the weight of the overburden reduces stress characterization to the determination of the magnitude and orientation of the maximum and minimum principal horizontal stresses, $S_{h\max}$ and $S_{h\min}$, respectively (Amadei & Stephansson, 1997), along with the determination of their trend with depth. Depending on the relative magnitudes of $S_{h\min}$, $S_{h\max}$, and S_v, different faulting regimes may be present such as normal, strike-slip, and thrust faulting (Anderson, 1951).

The vertical stress S_v is typically computed by integrating over the density log from the surface to a predetermined depth. The minimum horizontal stress, $S_{h\min}$, is estimated from pressure monitoring during hydraulic fracturing tests (if they propagate perpendicular to $S_{h\min}$) performed in isolated intervals (Fairhurst, 2003; Lin et al., 2008; Ljunggren et al., 2003; Schmitt et al., 2012). However, estimation of the maximum principal stress $S_{h\max}$ is somewhat challenging and associated with a significant amount of uncertainty. One approach is to assume that the rock is critically stressed and the rock strength behavior follows Mohr-Coulomb failure criteria with a friction coefficient between 0.6 and 1 and to compute the possible values for $S_{h\max}$ (Hickman & Davatzes, 2010; Zoback et al., 2003). This approach estimates a wide range of possible values for $S_{h\max}$. An alternative solution is to apply the width of borehole breakouts (Barton et al., 1988), which also relies on some assumptions and application of failure criteria. This approach results in $S_{h\max}$ estimates, which are primarily dependent on the used failure criterion (Valley & Evans, 2015). Typically, these estimates are applied to derive a first-order characterization by fitting a linear depth trend to the principal stress magnitudes (Cornet & Bérard, 2003; Valley & Evans, 2015).

Despite the magnitude estimations, the orientation of principal horizontal stresses may be estimated robustly from the borehole failures observed in image logs. The estimates of stress magnitudes from image logs require a number of assumptions that imply high uncertainties to the results. On other approach is to perform stress tensor analysis to explain the stress variability similar to Gao and Harrison (2018) and Lei and Gao (2018). Defining the stress tensor along deep boreholes using image logs is not possible, since they provide continuous information on some components of the stress tensor (not complete tensor). However, obtaining a full stress tensor is only achieved by overcoring, which gives the stress tensor on single points along the borehole (not a profile) and is not sufficient for stress-based tomography. Moreover, the stress measurements using overcoring also includes some variation (Martin, Read, Lang, 1990). Reliable information on the in situ stress is only achieved when a combination of all stress indicators (e.g., borehole images, overcoring, hydraulic fracturing and induced seismicity) is implemented (Stephansson & Zang, 2012).

In vertical boreholes, breakouts are aligned with the direction of minimum principal horizontal stress, $S_{h\min}$, and drilling-induced tensile fractures are formed in the direction of maximum principal horizontal stress, $S_{h\max}$ (Zoback et al., 2003). Figure 1a represents an example of a 360° view of an image log along the borehole GPK4 drilled at the Soultz-sous-Forêts EGS site in France, in which the natural fractures are regular sinusoids. Stress-induced features form as axial drilling-induced tension fractures (ADITFs) and en-echelon drilling-induced tension fractures (EDITFs). Figures 1b and 1c display the reflectivity image and borehole radius of a typical interval from the borehole drilled into Basel EGS, in which continuous borehole breakouts accompany a natural fracture.

Figure 2a shows the estimated profiles of $S_{h\min}$, $S_{h\max}$, and S_v based on hydraulic tests, borehole breakouts and density logs in the borehole drilled into Basel EGS. The detailed methodology to compute such profiles has been explained by Valley et al. (2014). Figure 2b displays the orientation of maximum horizontal principal stress orientation, $S_{h\max}$, inferred from the azimuth of borehole failure over successive 0.4 m windows on Basel borehole images. The deviation from the average $S_{h\max}$ orientation along the entire well (N144°, Valley & Evans, 2009) is presented in Figure 2b.

3. Methodology

3.1. Forward Simulation of Stress Variability in a Fractured Domain

In this chapter, we present the assumptions, the numerical code, and necessary information for simulating the geomechanical response and observed stress conditions in a fractured rock mass. For the sake of simplicity, we treat the problem as a 2-D plane strain case, that is, we expect a vertical planar section for the model containing a vertical borehole and cut by fractures with an infinite out-of-plane dimension. The rock mass is

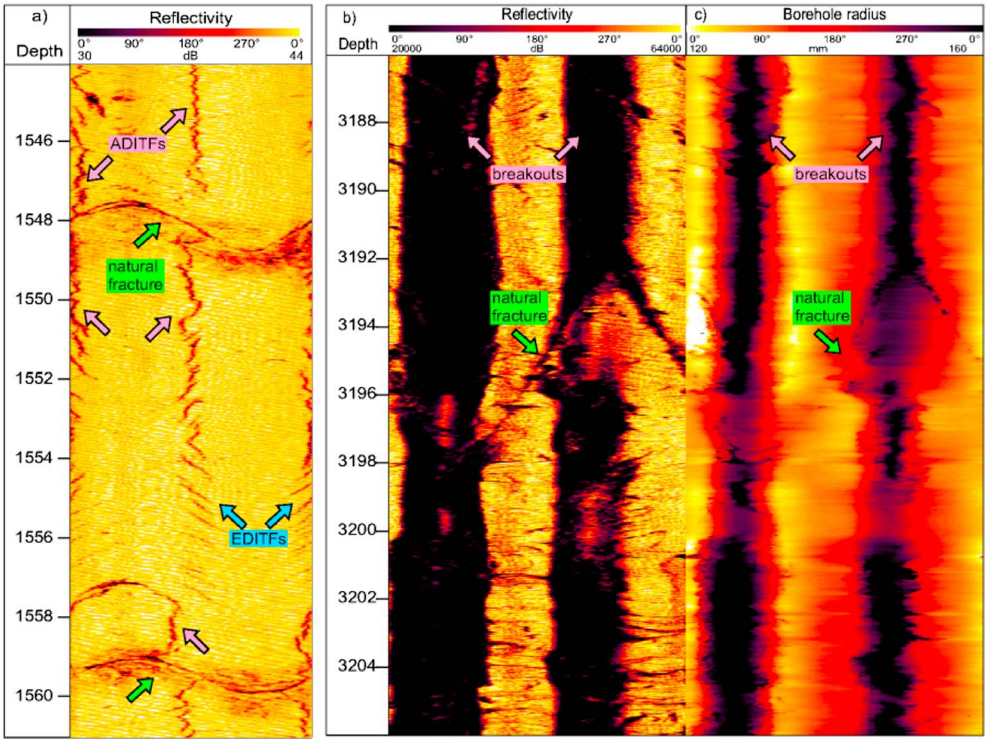

Figure 1. (a) A typical image log of GPK4 borehole drilled into Soultz-sous-Forêts Enhanced Geothermal System including the natural fractures and stress-induced fractures (axial drilling-induced tension fractures [ADITFs] and en-echelon drilling-induced tension fractures [EDITFs]); (b and c) an example of reflectivity and borehole radius from Basel-1 well, including borehole breakouts along with a natural fracture (Valley et al. 2014).

assumed to be isotropic and homogenous, and fractures are elastoplastic Mohr-Coulomb frictional interfaces that may slip due to applied far-field stresses.

The inversion process requires efficient and fast modeling of the stress variability induced by fractures within the rock mass. Conventional finite element codes are typically computationally demanding for modeling the mechanical response of a fractured rock mass under given stress conditions. Since the inversion process requires simulation of many realizations, we used a fast two-dimensional (2-D) simulator based on the displacement discontinuity method (DDM) developed by Jalali (2013). The DDM is an indirect boundary element method, which was developed by Crouch et al. (1983) based on an analytical solution to solve the finite line segment in an infinite body presented by Salamon (1963). This method was initially developed to model the mechanical behavior of thin underground excavations and then expanded for geomechanical modeling of fracture networks. Later on, the geomechanical simulator was coupled with a finite difference hydraulic simulator for hydromechanical modeling of fluid injection into fractured reservoirs (Jalali, 2013; Jalali & Valley, 2015). A good match has been obtained between numerical and analytical solutions such as the solutions presented by Sneddon (1951), Haimson (1968) and Detournay and Cheng (1991).

In the model, a fracture is discretized into multiple fractures segments, and any segment has two degrees of freedom: (1) normal and (2) shear displacement discontinuities. Induced displacement and stress at any point in the medium (including the fracture segments) can be estimated as a linear combination of all fracture segments' discontinuities. One must know the values of the discontinuities before the estimation of displacement and stress in the medium. The stress and displacement at each fracture segment (combination of in situ and induced) are written as a linear combination of all the fracture segment discontinuities. Fracture mechanics laws (here: Barton-Bandis model) are used then to derive the fracture segments' stress and displacement as a function of displacement discontinuities (Barton et al., 1985). The peak shear stress is estimated using a Mohr-Coulomb criterion and preshear elastic behavior. Beyond the peak shear stress, the fracture shear stiffness is taken as zero (sliding fracture). Dilation angle is considered as a constant that is dependent upon effective normal stress level during sliding and

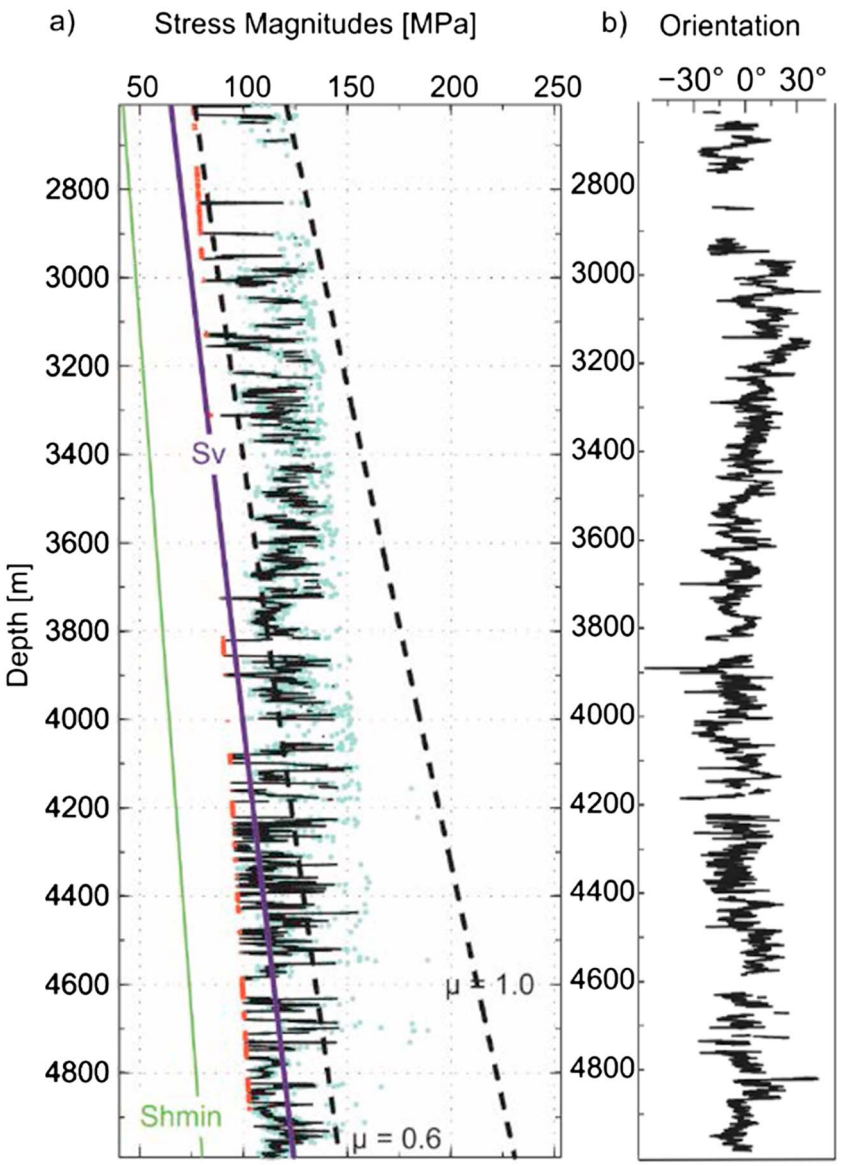

Figure 2. (a) Estimates of principal stress magnitudes in Basel Enhanced Geothermal System (Valley & Evans, 2015); (b) orientation of minimum principal horizontal stress inferred from breakouts in the borehole drilled into Basel Enhanced Geothermal System (Valley & Evans 2009).

otherwise is zero. Further details about the implementation of the DDM approach in the mechanical modeling of fractured rocks is provided by Jalali (2013).

Here we apply far-field stresses on the fractured domains and allow the fractures to slip to redistribute the stress within the entire domain. The simulator also returns the normal and shear displacements on each fracture planes. Then, we extract the stress fluctuations on a borehole in the center of the domain, which will be applied for DFN inversion.

Constraining far-field stresses from the current stress state inferred from borehole data is not straightforward. However, the variability on the stress measurements depends on scale and starts to minimize with the volume of rock mass (Martin, Read, Chandler, 1990). Thus, the average stress magnitude along the borehole would be a reasonable estimate of the far-field in situ stress. The current stress field can result from the superposition of successive tectonic phases. However, to keep the problem tractable, we assume that the current stress field has developed under a single loading event. In this study, for

Table 1
List of Input Parameters for Geomechanical Modeling of Fractured Rocks Using the DDM Simulator

Far-field principal stresses	Minimum principal stress horizontal	$\sigma_3 = -20$ MPa
	Maximum principal stress vertical	$\sigma_1 = -38$ MPa
Rock properties	Young's Modulus	$E = 60$ GPa
	Poisson's ratio	$v = 0.25$ MPa
Fracture properties	Normal stiffness	$K_n = 10^{11}$ Pa/m
	Shear stiffness	$K_s = 10^{10}$ Pa/m
	Cohesion	$c = 0$ MPa
	Friction angle	$\phi = 10^{\circ}$

illustrating the inversion procedure, we assume far-field stress of 20 MPa horizontal and 38 MPa vertical stress on the 2-D DFNs with zero shear stress. As a relatively short vertical extent is considered in the model, we neglect the gravity-driven stress magnitude increasing with depth.

The simulator requires the definition of rock and fracture properties based on available information from geophysical logging and laboratory tests on cores. The required information on these properties is assumed constant in the inversion process (listed in Table 1). The fracture stiffness is difficult to constrain (both shear and normal). However, its impact is limited if plastic slip occurs. Thus, stiffness is considered constant during the inversion.

To ensure the slip-on fracture planes in every case, a low friction angle of $\phi = 10°$ is selected. The geomechanical simulator delivers the stress redistribution within the network at every point (horizontal, vertical and shear stresses). Here we define a parameter β, which indicates the orientation of maximum principal stresses from the vertical borehole (positive clockwise). This parameter is computed using the following equation:

$$\tan(2\beta) = \frac{2\tau}{\sigma_{yy} - \sigma_{xx}} \tag{1}$$

where τ represents the shear stress, σ_{yy} is vertical stress, and σ_{xx} denotes the horizontal stress at any point along the borehole.

3.2. Principles of Bayesian Inversion

A Bayesian inversion framework is used to fit the DFN models to the observed stress measurements. In general, Bayesian inference aims to provide a probabilistic model to a set of unknown parameters and deliver a probabilistic characterization of unknown model parameters. The posterior probability distribution is computed based on an available prior collection of information and the likelihood of observations (Gelman et al., 2014). Bayesian inversion has been applied to related geological problems such as for reconstruction of the stress field (Lecampion & Lei, 2010) and characterization of flow and transport in heterogeneous media (Lee & Kitanidis, 2013; Mondal et al., 2010). The Markov Chain Monte Carlo (MCMC) method is one of the most common techniques of Bayesian inference in geosciences. MCMC has been applied to solve inverse problems using various sources of information such as seismic tomography (Bodin et al., 2012), tracer tomography (Jiménez et al., 2016), and fracture network intersections with boreholes (Mardia et al., 2007). The transdimensional reversible jump Markov Chain Monte Carlo is a unique variant of MCMC, in which the number of parameters can vary among subsequent iterations during the inversion process. Somogyvári et al. (2017) introduced this inversion approach for calibrating orientation, lengths, and numbers of fractures in DFNs using cross-well tracer tomography experiments. That work is also the basis for the presented stress-based inversion procedure, but we keep the number of fractures during the inversion fixed.

3.3. Inversion Methodology

The stress-based tomography requires at least two components of in situ stress (one magnitude and one orientation). Preliminary analysis shows that one single stress orientation is not sufficient to reconstruct simple DFNs with a very small number of fractures (presented in supporting information). Two stress components, for example, the orientation of minimum principal stress (observation 1) and one magnitude among $S_{h\min}$, $S_{h\max}$, and S_v (observation 2) is sufficient for solving the inverse problem. However, estimates of all three quantities are still required for defining the far-field stress in this analysis (as discussed in section 3.1).

3.3.1. Prior Information on Fracture Network

The inversion procedure requires prior knowledge of the statistical distribution of fracture attributes within the study domain. The fundamental understanding of the fracture length distribution is a prerequisite to populate the initial DFN in the inversion process (Figure 3). Fracture length (l) distribution in geological formations has been reported to follow power law distributions on different scales like $n(l)\,\mathrm{d}l = c\ l^{-a}\,\mathrm{d}l$, where a is the length exponent and c is a constant of normalization. The power law exponent of the fracture length

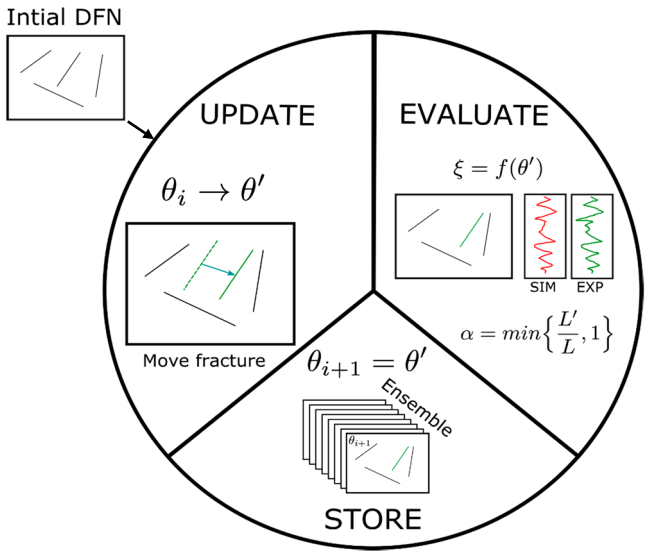

Figure 3. Overview of the Markov Chain Monte Carlo algorithm: θ denotes the model vector, θ_i is the last accepted model, θ' is the proposed model, ξ is the observation vector (the stress measurements), $f(\theta)$ is the forward model, α is the Metropolis-Hastings acceptance criteria, and L is the likelihood function. The initially generated discrete fracture network (DFN) goes into the loop, and the DFN is updated by the movement of a randomly selected fracture. Each realization is evaluated using Metropolis-Hastings criteria (SIM is the simulated stress perturbation; EXP is the observed or expected stress perturbation), and any accepted realization is stored in the ensemble. The ensemble is finally converted to a probability map using the methodology described in section 5.1.

distribution in 2-D outcrops is typically between 1.5 and 3.5 (Bonnet et al., 2001; Torabi & Berg, 2011). Also, the fracture positions on the specified borehole may be inferred from image logs. The fractures cutting the borehole compute the minimum fracture spacing in each set. However, the location of fractures along the borehole is not fixed in this study. Moreover, the orientation of fractures in deep boreholes mostly belong to two dominant fracture sets (Valley, 2007; Ziegler et al., 2015), which may be considered as prior information and invariant in the inversion process.

3.3.2. Inversion Procedure

In Bayesian inference, data are handled as random variables with given probability density functions (PDF). Hence, the inverse problem can be expressed using Bayes' theorem as

$$P(\theta|\xi) = \frac{L(\xi|\theta)P(\theta)}{P(\xi)} \tag{2}$$

where $P(\theta|\xi)$ denotes the posterior probability of the inverse problem (the target distribution, i.e., the probability of a model parameter θ given the observation data of ξ). $L(\xi|\theta)$ is the likelihood function (the probability of an observation vector ξ given the model parameter vector θ), $P(\xi)$ is the observation probability, and $P(\theta)$ is the prior information.

If we consider that stress observations (orientation and magnitude at a given borehole) follow a normal distribution, the likelihood function can be written as

$$L(\xi|\theta) = \frac{1}{\sqrt{4\pi\sigma^2}} \exp\left(-\frac{(\xi - f(\theta))^2}{4\sigma^2}\right) \tag{3}$$

where σ^2 is the variance of the normal distribution and $\xi(\theta)$ is the forward model for the simulation of the stresses. This function is equivalent to computing a root-mean-squared misfit (Aster et al., 2005). In this work, we use multiple types of observations together, and thus, the used likelihood function is the product of numerous normal distributions. The sensitivity of the inversion toward the different observations can be tuned by the variance values. In simple words, the likelihood function is computed using equation (3) for both observations of stress orientation and magnitude and then summed up. Since the M-H criteria is multidimensional, one can define many parameters to do the inversion process like treating the stress as a tensor along the borehole. Although this may result in better inversion results, but in case of EGS, obtaining a full stress tensor along the borehole is difficult.

In equation (2), $P(\theta)$ represents the prior, that is, the information known about the model parameters before the inversion. The prior information here is mainly used to generate the initial solution of the inversion. $P(\xi)$ is the probability of observations, which could be written as the following marginal distribution over the complete model space:

$$P(\xi) = \int L(\xi|\theta)P(\theta)\mathrm{d}\theta \tag{4}$$

This marginal distribution is not a function of the models, and thus, it can be considered constant throughout the inversion. The posterior probability function cannot be expressed in an analytical form, but it can be calculated for specific models. MCMC uses this property, as it calculates the target distribution as particular models. The main idea behind MCMC is to create a Markov chain with a stationary distribution that matches the target distribution, the posterior. This is obtained by specifying a transition kernel, which is a set of rules to create the next chain element from the previous one ($\theta_i \rightarrow \theta'$). A random update to propose a new model parameter vector (θ') with the probability $q(\theta_i \rightarrow \theta')$ is chosen here. We use the Metropolis-Hastings algorithm, where this update step has to be reversible, and thus, the update $q(\theta' \rightarrow \theta_i)$ must be realized by a probability value, too. Reversibility ensures the stationarity of the Markov chain. The workflow and implementation of the algorithm are presented in Figure 3.

Table 2
Geometrical Characteristics of Test Cases

Cases	Simple synthetic network		Outcrop-based network	
Fracture set	Set 1	Set 2	Set 1	Set 2
Fracture orientation from the vertical borehole (positive clockwise)	45°	−45°	30°	−65°
Minimum spacing	10 m	10 m	2.55 m	2.5 m
Fracture length exponent (α)	1.5		2.6	
Minimum fracture length	40 m		8 m	
Total fracture length	250 m		220 m	
Domain size	100×100 m^2		50×40 m^2	

The initial fracture network is generated randomly using a known power law length distribution with a given minimum fracture spacing (Somogyvári et al., 2017). This initial solution is then entered in the iterative MCMC algorithm. During each subsequent iteration, one fracture is randomly selected, then a new fracture center is drawn from a uniform distribution over the area of investigation. Subsequently, the forward model is simulated with the updated DFN realization. The acceptance probability of a proposed model realization is calculated as

$$\alpha(\theta', \theta_i) = \min\left\{\frac{L(\xi|\theta')}{L(\xi|\theta_i)}\frac{p(\theta')}{p(\theta_i)}\frac{q(\theta' \to \theta_i)}{q(\theta_i \to \theta')}, 1\right\} \tag{5}$$

This expression is known as the Metropolis-Hastings acceptance criterion (Geyer, 2011). It depends on the ratio of the likelihoods and the priors, as well as the ratio of the probability of the reverse and the forward proposal step. The calculation of this ratio is more straightforward than calculating the individual posteriors as there is no need to estimate the marginal distribution of the observations anymore. Because the fracture movement update uses the same uniform distribution, the probabilities $q(\theta' \to \theta_i)$ and $q(\theta_i \to \theta')$ are the same, and the acceptance criterion simplifies to

$$\alpha(\theta', \theta_i) = \min\left\{\frac{L(\xi|\theta')}{L(\xi|\theta_i)}\frac{p(\theta')}{p(\theta_i)}, 1\right\} \tag{6}$$

This version of MCMC is known as the random-walk Metropolis-Hastings algorithm (Brooks et al., 2011). After the acceptance criterion is calculated, a random number from the interval [0, 1] is drawn and compared to α. If the drawn number is smaller, the proposed realization gets accepted. This is equivalent to the update being accepted with a probability α. The accepted realization gets stored (otherwise, the last accepted model is kept), and the next iteration starts with its random update. The stored set of model realizations is called the ensemble, which is the result of the MCMC simulation. The first half of the ensemble is discarded to remove the bias of the initial model choice, *t*. The ensemble thus represents the investigated posterior probability distribution, and not only one calibrated model realization.

4. Test Cases

We test the methodology by reconstructing two synthetic fracture networks with known geometry (i.e., given position, orientation, and length distribution of the fractures). The first case is a simple synthetic fracture network built up by a few fractures, and the second case presents a more complex and realistic fracture network mapped from outcrop field data. Table 2 represents the geometrical characteristics of both DFNs of the test cases. Both are described by two fracture sets.

4.1. Simple Synthetic Network

This case contains four large fractures from two orthogonal orientations within a domain of 100×100 m^2. The minimum spacing between fractures of the same sets is 10 m, the minimum length of the fractures is 40 m, and the total length within the domain is 250 m. It is possible to run the inversion process without defining a minimum spacing, but the MCMC needs larger number of inversion runs to converge to a common statistical distribution, whereas it is not possible to run the inversion process without a minimum fracture length. Although there is not a real limit in the nature, but the definition of power law distribution requires the

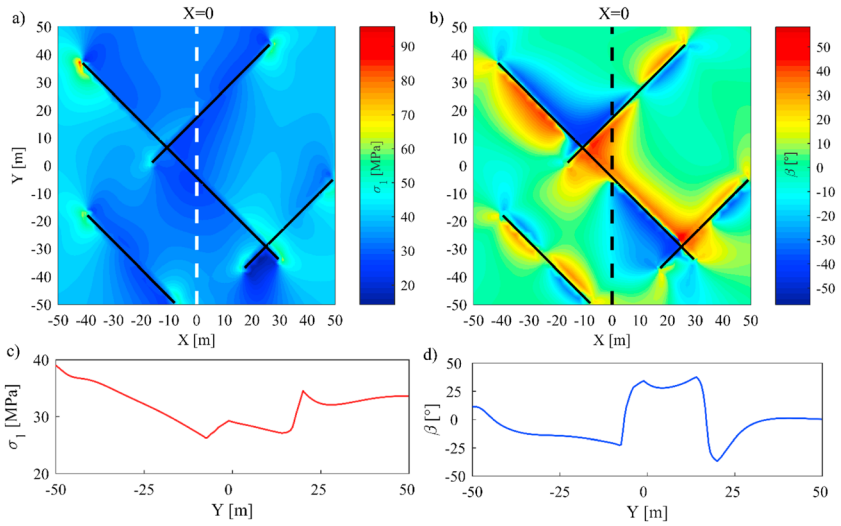

Figure 4. Forward simulation of stress variability within the simple synthetic network given the geometrical characteristics listed in Table 2, and using input parameters for the geomechanical model from Table 1. (a) The σ_1 field and (b) the β field. Stress magnitude and orientation profiles representing the stress fluctuations along the borehole ($X = 0$) are shown in c) and d).

definition of a range with a constant slope in log-log space. This range requires a minimum and maximum fracture length. Since we know the fracture length exponent (e.g., from literature or outcrop data), then it is necessary to define the minimum fracture length to the algorithm. Moreover, Valley et al. (2014) performed a sensitivity analysis on the parameters affecting the stress perturbation due to slip on a single fracture. They found that the stress variability is largely dependent on the fracture length. Thus, smaller fractures do not have a large impact on the stress variability, particularly when they do not cross the borehole.

Before starting the inversion procedure, we need to simulate the stress variability within the domain and extract the stress profiles along the predefined borehole. Here the borehole is placed in the center of the domain. Figures 4a and 4b present the σ_1 and β variations within the synthetic network domain $[-50, 50]$ due to fracture slip loaded by the far-field stresses defined above. The simulation parameters are listed in Table 1. The borehole is situated in the center of the domain ($X = 0$) parallel to the Y axis, and here the simulated stress profiles are extracted. These profiles, shown in Figures 4c and 4d, are computed at 50-cm resolution along the borehole (i.e., based on 201 data points in the borehole). To summarize, we aim at reconstructing the DFN geometry in Figure 4a by using these two stress profiles and prior information listed in Tables 1 and 2.

4.2. Outcrop-Based Network

This case represents a more complex fracture network, which is based on outcrop field data. This fracture network is mapped from Tschingelmad crystalline outcrop in upper Aar valley in Grimsel region of Central Alps, Switzerland (Ferrari et al., 2017; Ziegler et al., 2013; Ziegler et al., 2014). For a detailed description of the geological settings in the given area, we refer to the previous references. Figure 5a represents a schematic view of the geological model of the mapped area, and Figure 5b shows the mapped fracture network. We selected an area of 50×40 m^2 for this analysis and mapped the fractures with a minimum length of 8 m. The fractures in this area belong to two primary fracture sets. Their orientations are approximately 30° and −65° from the vertical axis (positive clockwise).

The network of Figure 5b follows a power law length distribution with an exponent of 2.6 and a cut-off at a length of about 8 m. Since the large fractures are of highest importance to the hydromechanical response of fractured rocks (Baghbanan & Jing, 2007; Darcel, Bour, Davy, & De Dreuzy, 2003; de Dreuzy et al., 2001), we ignore the fractures smaller than the cut-off length. A power law length exponent is derived by fitting a power law distribution to the histogram of fractures within the domain as illustrated in Figure 5c. The corresponding probability density function of the mapped network thus reads as $p(l)\ \mathrm{d}l = 0.16\ l^{-2.6}\ \mathrm{d}l$. A power law is fit to the whole fracture network (without any cut-off) so that robust estimates of the constants in this equation are created. This probability density function is required to define the initial DFN realization.

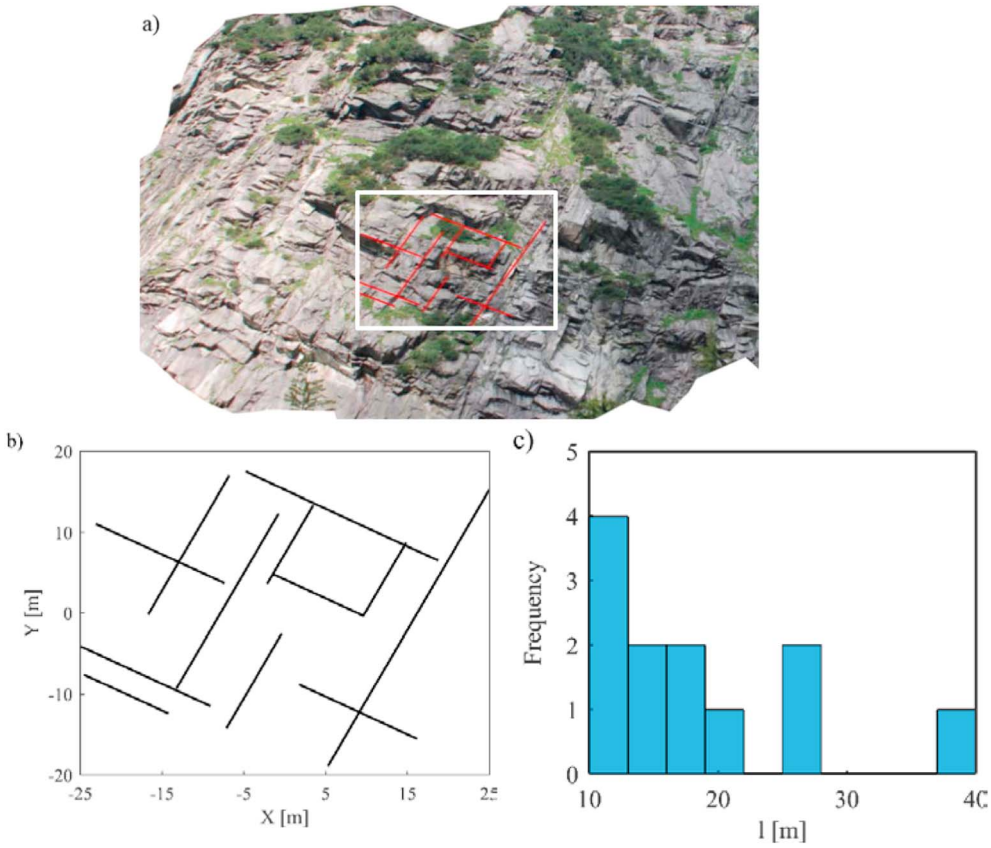

Figure 5. (a) Surface geological model of the Tschingelmad outcrop; (b) fracture network mapped from the geological model. Only the fractures larger than the predefined cut-off (8 m) are mapped; (c) histogram of fracture length distribution, $p(l)\ dl = 0.16\ l^{-2.6}\ dl$.

Similar to the synthetic case, we first simulate the stress variability induced by fractures, when far-field stresses are applied. The simulation parameters are the same as for the simple synthetic case. Then, we place a borehole in the center of the domain at $X = 0$ (parallel to Y axis) and extract the stress heterogeneities along it. Figures 6a and 6b represent the resulting magnitude σ_1 and orientation β fields within the entire

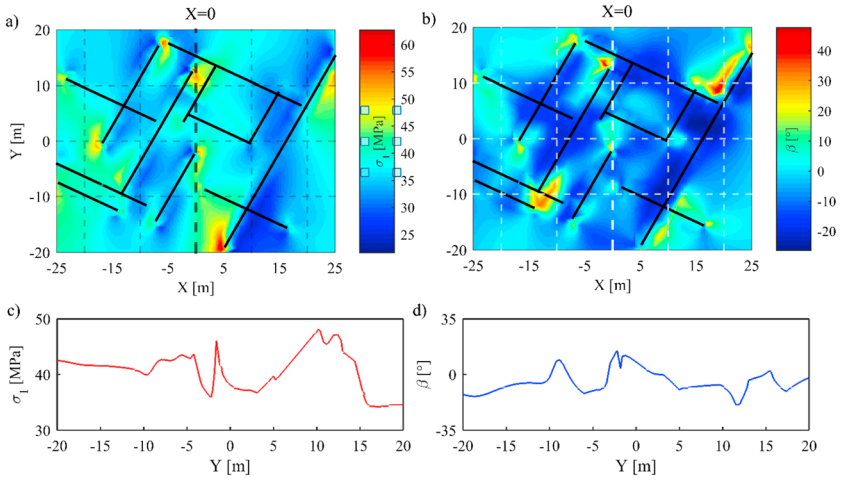

Figure 6. Forward simulation of stress variability within the outcrop-based fracture network with the characteristics listed in Table 2 and input parameters of the geomechanical model from Table 1, (a) σ_1 field and (b) β field. Profiles representing the variability are depicted in (c) σ_1 and (d) β at $X = 0$.

domain, respectively. Figures 6c and 6d show the σ_1 and β profiles computed at every 20-cm along the borehole (to have 201 data points in the borehole similar to the hypothetic case). The inversion procedure aims at reconstructing the DFN geometry in Figure 5b using these stress profiles and prior knowledge on the rock mass and fracture network presented in Tables 1 and 2.

5. Results

An essential question of MCMC methods is when to stop the sequential simulations or, in other words, when the sampling can be considered complete? Here we followed the recommendations by Gelman et al. (2004) to check the convergence of individual parameters until they converge to a joint distribution. The inversion process provided a large number (more than 100 for the simple synthetic case and more than 1,000 for the outcrop-based case) of accepted DFN realizations. As a standard practice, the first half of the chain was considered as the burn-in period and discarded (Geyer, 2011) to eliminate the effects of the initial model, and not considered for visualization of the ensemble.

Straightforward ways of visualizing features of a final ensemble are plotting exemplary DFN realizations or taking the mean of all geometric parameters, but these would significantly reduce the real information content of the ensemble. The resulting ensemble is more than just a collection of plausible solutions, but it is the representation of the posterior probability function. Another approach is to extract higher-order statistical properties of the individual DFN parameters, which however, may obscure spatial correlation of results. Instead, a fracture probability map as presented by Somogyvári et al. (2017) was derived for each case. Such a map is created by rasterizing the individual DFN realizations and then stacking these together. The local probabilities are calculated pixel by pixel, based on the frequency of fracture occurrence. The full map depicts the probabilistic location and length of fractures within the study domain; it can easily be analyzed visually and may be used for further analyses.

5.1. Simple Synthetic Case

Here we first explain the results for the synthetic case. First of all, a random DFN realization (known as initial DFN) with the geometrical properties listed in Table 1 was generated. The initial DFN for the inversion process of the simple synthetic case is presented in the supporting information. The MCMC algorithm applied the stress profiles in Figures 3c and 3d as the observation profiles to reconstruct the initial fracture network geometry of Figure 4a. The Markov sequence kept moving the fractures inside the domain while respecting the minimum spacing of fractures in each set. It compared each realization-specific stress profile at $X = 0$ with the *true* one of Figure 4 to assess the misfit. When the updated DFN met the Metropolis-Hastings acceptance criteria, the DFN was stored in the ensemble. We let the MCMC algorithm run 24 hr on an office PC (single thread, Intel® Core i7™-6700k 4 × 4.0 GHz).

Since the DFN is not complex, the MCMC algorithm converged to the initial DFN relatively fast. Figure 7a shows that there is a rapid misfit decrease after the first 50 accepted realizations and the computed misfit remains relatively constant after that. However, the ensemble size may be significant and include a large number of parameters. For the presentation of the posterior distribution, a subset of the converged range is selected as the final ensemble, and as outlined above the first half of realizations discarded.

Figures 7b and 7c compare the hypothetic case with the probability map derived from the visualization of the obtained ensemble. The light colors in Figure 7c denote the most probable locations of the fractures, while the black color indicates that no fracture is present. Figure 7c reveals that the inversion recognizes well the location and length of the fractures within the network, although they are not intersecting the borehole in the middle. However, the fractures that do not cross the borehole are recognized with a lower probability (larger uncertainty). Since the longer fractures have the highest influence on the stress heterogeneity (Valley et al., 2014), they are most accurately located within the domain.

Now, we choose a random DFN from the selected range and compute the stress profiles (σ_1 and β) at the borehole along $X = 0$. Figures 8a and 8b compare the stress profiles of this DFN with that of the original DFN. The close match between the two stress profiles is similar also for the other realizations of the ensemble, and it demonstrates successful inversion.

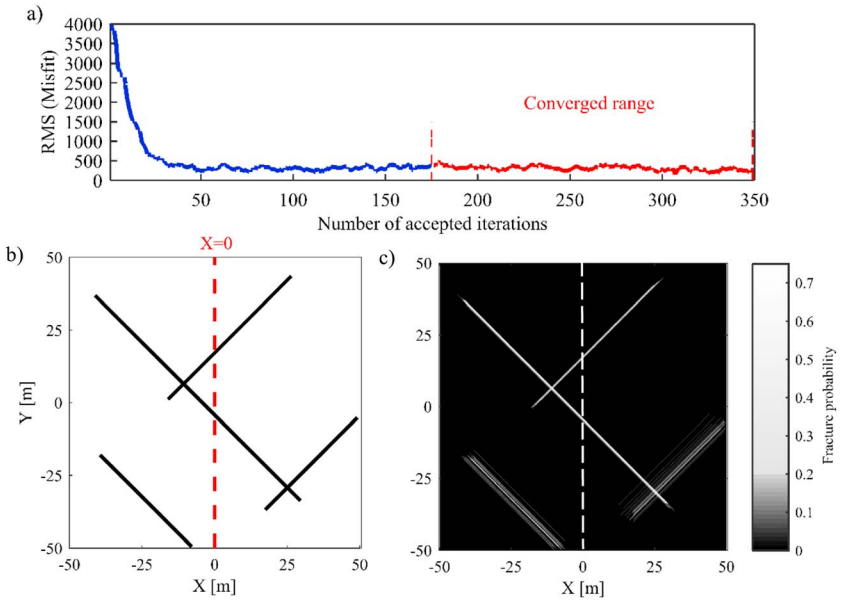

Figure 7. (a) Misfit evolution of all accepted realizations during the Markov Chain Monte Carlo sampling. The converged range is chosen to be between the 175th and 350th iteration; (b) the real synthetic network; (c) the fracture probability map of the entire accepted range. RMS = root-mean-square.

5.2. Outcrop-Based Case

The inversion of the outcrop-based network (Figure 5b) was initiated by sampling from a power law length distribution in a domain of 50×40 m^2. We applied a probability density function of $p(l)\ dl = \ 0.16\ l^{-2.6}\ dl$ with a minimum length of 8 m. The initial DFN was generated using the key geometrical characteristics in Table 2. The locations of fractures were assumed to be distributed uniformly within the domain respecting the minimum spacing of each fracture set. The fractures belong to two main families with angles of $-65°$ and 30° from vertical (Table 2). Equivalent to the procedure for the synthetic case, the MCMC inversion procedure continuously moved the fractures in DFNs for 24 hr. The same inversion methodology was employed to reconstruct the DFN with the two stress profiles (i.e., observations) of Figures 6c and 6d. The initial DFN for the inversion process of the simple synthetic case is presented in the supporting information.

Figure 9a depicts the evolution of misfit during the inversion process. The full MCMC sampling procedure accepted approximately 10,000 realizations. In comparison to the more straightforward synthetic case, the MCMC algorithm converged slower and required at least 1,000 iterations to achieve a relatively constant misfit. If half of the initial iterations are discarded, the converged range is between the 5,000th–10,000th iterations. As the target DFN and the associated inversion problem became more complicated, the mean misfit of the converged range (684) became more than double that of the simple hypothetical case (311). Since the converged range consisted of many similar realizations and to accelerate visualization, the final ensemble was thinned.

Figures 9b and 9c compare the original DFN with the probability map. The probability map shows that the inversion again is sensitive to the most extended fractures. This is expected, because long fractures have a substantial impact on stress heterogeneities, even if they do not cut the borehole. Even though the probability map shows that also some smaller features are adequately imaged, some fractures are not well reconstructed or appear blurred in the map.

Figures 10a and 10b compare the initial stress profiles of Figures 6c and 6d with the profiles of an arbitrary realization of the final ensemble. There is a substantial similarity between the original and reproduced stress profile for both σ_1 and β. However, because of the higher complexity, the match is not as excellent as for the synthetic case. The most considerable discrepancy is associated with the stress heterogeneity induced by a fracture tip at $Y = -1.8$ m (black circle on the σ_1 profile, Figure 9a). This is mainly due to the fracture tip, which is very close to the borehole and which affects more the profile of σ_1 than of β. Although the location of this

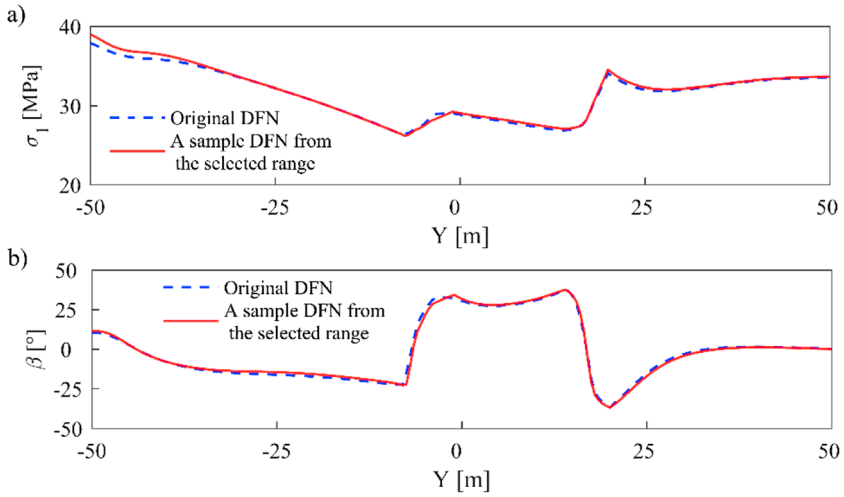

Figure 8. (a) Profiles of stress magnitude σ_1 and (b) orientation β at the borehole for the simple synthetic case (Figures 4c and 4d) compared to profiles at the same location of a randomly chosen discrete fracture network (DFN) from the selected range in Figure 7a.

fracture has been identified in the probability map, its reconstructed length is not sufficient to generate a peak in the stress profile.

To reproduce stress variabilities comparable to the stress profiles in deep boreholes, we assumed a relatively low friction angle in both synthetic and outcrop-based fracture networks. Since the friction angle of crystalline rocks lies typically between 30° and 45°, we tested the inversion approach with a friction angle of 35° with the same inversion parameters (presented in the supporting information). The inversion results revealed that although the higher friction angles may result in less variability on the stress profiles; the corresponding stress variability still could reconstruct the significant features of the fracture network.

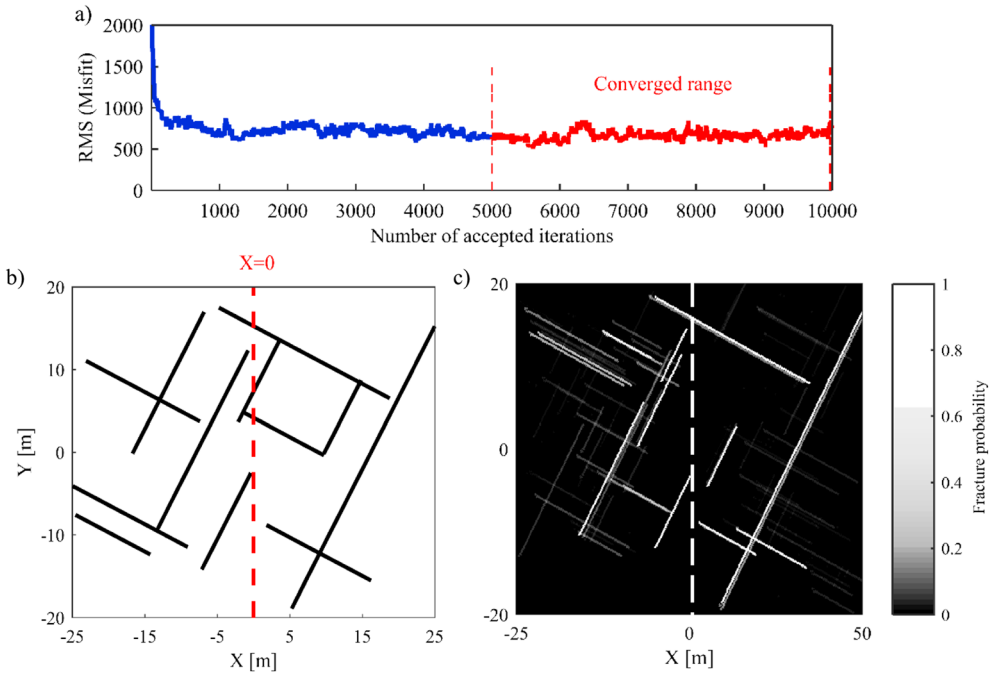

Figure 9. (a) Markov Chain Monte Carlo convergence trend of accepted realizations for the outcrop-based fracture network; (b) the original true network compared to (c) the corresponding fracture probability map obtained by inversion.

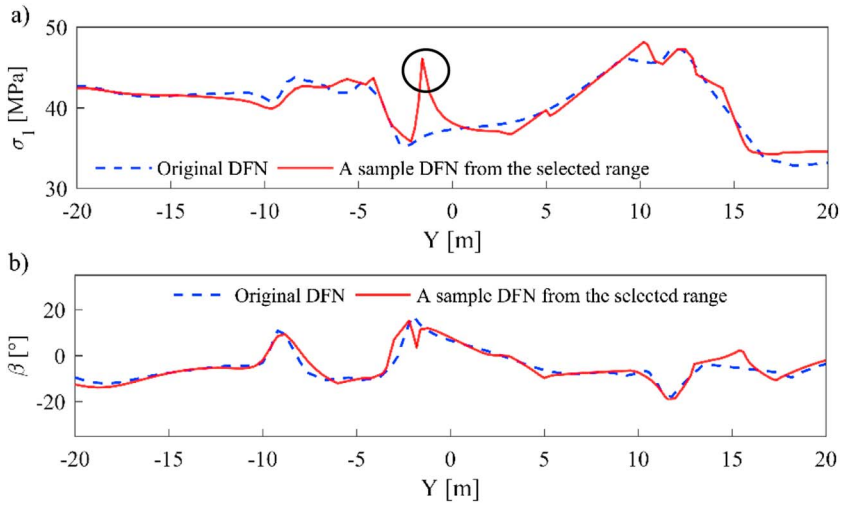

Figure 10. Stress profiles of the initial outcrop-based model compared to those of a randomly sampled discrete fracture network (DFN) of the final ensemble. The black circle indicates the part of the stress profile most profoundly affected by a fracture tip and which is not well reproduced.

6. Discussion and Conclusions

Fracture network characterization has been a challenge in many different engineering applications such as EGS developments. A robust recipe for extracting the fracture network geometry from available data including geological, geophysical, and hydrogeological investigations is still lacking. However, stochastically generated fracture networks may be constrained by measured information. Borehole image logs provide valuable information on the fluctuations of in situ stress components (e.g., maximum principal stress and its orientation) along the wellbore, if borehole breakouts or drilling induced tensile fractures are present. Since in situ stress fluctuations are strongly influenced by the slip on natural fractures in the past, they also carry information on geometrical aspects of fracture networks. This is exploited in the presented example application based on a new Bayesian approach, also referred to as stress-based tomography, which flexibly adjusts fracture networks to match single borehole stress profiles.

Comparing for the two examples the initial DFNs and the obtained probability maps reveals that significant features are accurately determined. Even if some fractures do not intersect the borehole, their impact may be significant on the observed stress heterogeneities. This effect is sufficient for imaging such relatively long *hidden* fractures in the vicinity of a borehole. This may not be enough for reconstructing smaller fractures if they are far from the borehole. Furthermore, in some instances, the probability map may not well resolve regions of higher local fracture intensity although roughly indicating the presence of such areas. Thus, this inversion methodology is more sensitive to longer fractures than to smaller ones. Note that since larger fractures often represent the major pathways for fluid flow and yield higher seismic magnitudes, they are also more critical for case-specific performance, hazard and risk assessments.

One limitation of this approach originates from the difficulty to constrain the fracture strength properties such as normal and shear stiffness. Therefore, it is suggested to test different strength parameters before the inversion process and choose a reliable estimate based on the observation profiles. Analyzing the effect of these parameters on the inversion will be subject to future development of this approach.

One possible additional development of the presented stress-based tomography is to include further complementary field information such as tomographic information from geophysical measurements, tracer or hydraulic tomography (Brauchler et al., 2013; Dorn et al., 2011; Zha et al., 2015). The future development of this research will include the data from multiple boreholes (to be developed) and comparison to other tomographical approaches (i.e., geophysical, hydraulic, and tracer). Joint inversion of different data in the MCMC procedure could impose extra constraints on the generation of the probability maps. This could yield improved capabilities for reconstruction of more complex DFNs and of three-dimensional (3-D) features. However, practical applications of this approach requires the development of a robust, efficient, and fast

geomechanical simulator in three dimensions. Data collected in deep underground laboratories with extensive characterization of the stress field and fracture network could be an excellent opportunity to further develop and test the approach.

In the presented approach, the prior knowledge of 2-D fracture length distribution is an input for the inversion process. However, this information may not be available. Since fracture length exponents in geological media are typically between 1.5 and 3.5, one option is to initialize (i.e., generate initial DFNs of) the MCMC algorithm with some length of exponents within this range. The length exponent associated with the lowest misfit would be most suitable for creating the probability map. Also, in the present implementation, the fracture intensity (i.e., fracture numbers) is assumed to be known a priori (by defining a constant *c* for the length distribution and a minimum length). Thus, one further development of the presented approach is to implement a transdimensional inversion (Somogyvári et al. (2017)), in which the number of fractures is treated as a decision variable.

Acknowledgments
The research leading to these results has received funding from the European Community's Seventh Framework Program under grant agreement 608553 (Project IMAGE). P. Bayer acknowledges support by the German Research Foundation (BA2850/5-1). The data leading to the results of this paper are attached as supporting information (dataset). The data include the stress profiles (required for the inversion process) and the resulting tomograms (probability maps) of studied cases.

References

Achtziger-Zupančič, P., Loew, S., & Mariéthoz, G. (2017). A new global database to improve predictions of permeability distribution in crystalline rocks at site scale. *Journal of Geophysical Research: Solid Earth*, *122*, 3513–3539. https://doi.org/10.1002/2017JB014106

Afshari Moein, M. J. (2018). *Linkage between fracture network, stress heterogeneities and induced seismicity in deep geothermal reservoirs* (Doctoral Dissertation). Zurich: ETH Zurich.

Afshari Moein, M. J., Tormann, T., Valley, B., & Wiemer, S. (2018). Maximum magnitude forecast in hydraulic stimulation based on clustering and size distribution of early microseismicity. *Geophysical Research Letters*, *45*, 6907–6917. https://doi.org/10.1029/2018GL077609

Amadei, B., & Stephansson, O. (1997). *Rock Stress and its Measurement*. London: Chapman and Hall.

Amann, F., Gischig, V., Evans, K., Doetsch, J., Jalali, R., Valley, B., Krietsch, H., et al. (2017). The seismo-hydro-mechanical behaviour during deep geothermal reservoir stimulations: Open question tackled in a decameter-scale in-situ stimulation experiment. *Solid Earth Discussions*, *1*, 2017–2079. https://doi.org/10.5194/se-2017-79

Anderson, E. M. (1951). *The dynamics of faulting and dyke formation with applications to Britain*. Hafner Pub. Co.

Aster, R. C., Borchers, B., & Thurber, C. H. (2005). *Parameter Estimation and Inverse Problems*. Boston: Elsevier.

Baghbanan, A., & Jing, L. R. (2007). Hydraulic properties of fractured rock masses with correlated fracture length and aperture. *International Journal of Rock Mechanics and Mining Sciences*, *44*(5), 704–719 https://doi.org/10.1016/j.ijrmms.2006.11.001

Barton, C. A., & Zoback, M. D. (1994). Stress perturbations associated with active faults penetrated by boreholes: Possible evidence for near-complete stress drop and a new technique for stress magnitude measurement. *Journal of Geophysical Research*, *99*(B5), 9373–9390. https://doi.org/10.1029/93JB03359

Barton, C. A., Zoback, M. D., & Burns, K. L. (1988). In-situ stress orientation and magnitude at the Fenton geothermal site, New Mexico, determined from wellbore breakouts. *Geophysical Research Letters*, *15*(5), 467–470. https://doi.org/10.1029/GL015i005p00467

Barton, N., Bandis, S., & Bakhtar, K. (1985). Strength, deformation and conductivity coupling of rock joints. In *International journal of rock mechanics and mining sciences & geomechanics abstracts* (Vol. 3, pp. 121–140). Elsevier.

Berrone, S., Canuto, C., Pieraccini, S., & Scialò, S. (2017). Uncertainty quantification in Discrete Fracture Network models: Stochastics geometry. *Water Resources Research*, *54*, 1338–1352. https://doi.org/10.1002/2017WR021163

Blake, K., & Davatzes, N. C. (2011). Crustal stress heterogeneity in the vicinity of Coso Geothermal Field, CA. In *Proceedings, Thirty-Sixth Workshop on Geothermal Reservoir Engineering* (p. 11). Coso, CA.

Bodin, T., Sambridge, M., Tkalčić, H., Arroucau, P., Gallagher, K., & Rawlinson, N. (2012). Transdimensional inversion of receiver functions and surface wave dispersion. *Journal of Geophysical Research*, *117*, B02301. https://doi.org/10.1029/2011JB008560

Bonnet, E., Bour, O., Odling, N. E., Davy, P., Main, I., Cowie, P., & Berkowitz, B. (2001). Scaling of fracture systems in geological media. *Reviews of Geophysics*, *39*(3), 347–383. https://doi.org/10.1029/1999RG000074

Brauchler, R., Hu, R., Hu, L., Jiménez, S., Bayer, P., Dietrich, P., & Ptak, T. (2013). Rapid field application of hydraulic tomography for resolving aquifer heterogeneity in unconsolidated sediments. *Water Resources Research*, *49*, 2013–2024. https://doi.org/10.1002/wrcr.20181

Brooks, S., Gelman, A., Jones, G., & Meng, X.-L. (2011). *Handbook of Markov Chain Monte Carlo*. Boca Raton, FL: CRC Press.

Cornet, F. H., & Bérard, T. (2003). A case example of integrated stress profile evaluation. In K. Sugawara, Y. Obara, & A. Sato (Eds.), *3rd International Symposium on Rock Stress* (pp. 23–24). Brookfield, Vt: A. A. Balkema.

Crouch, S. L., Starfield, A. M., & Rizzo, F. (1983). Boundary element methods in solid mechanics. *Journal of Applied Mechanics*, *50*(3), 704. https://doi.org/10.1115/1.3167130

Darcel, C., Bour, O., Davy, P., & De Dreuzy, J. (2003). Connectivity properties of two-dimensional fracture networks with stochastic fractal correlation. *Water Resources Research*, *39*(10), 1272. https://doi.org/10.1029/2002WR001628

Darcel, C., Bour, O., & Davy, P. (2003). Stereological analysis of fractal fracture networks. *Journal of Geophysical Research*, *108*(B9), 2451. https://doi.org/10.1029/2002JB002091

Davatzes, N. C., & Hickman, S. H. (2010). Stress, fracture, and fluid-flow analysis using acoustic and electrical image logs in hot fractured granites of the Coso geothermal field, California, USA

Davies, R., Foulger, G., Bindley, A., & Styles, P. (2013). Induced seismicity and hydraulic fracturing for the recovery of hydrocarbons. *Marine and Petroleum Geology*, *45*, 171–185. https://doi.org/10.1016/j.marpetgeo.2013.03.016

Day-Lewis, A., Zoback, M., & Hickman, S. (2010). Scale-invariant stress orientations and seismicity rates near the San Andreas fault. *Geophysical Research Letters*, *37*, L24304. https://doi.org/10.1029/2010gl045025

de Dreuzy, J.-R., Davy, P., & Bour, O. (2001). Hydraulic properties of two-dimensional random fracture networks following a power law length distribution 1. Effective connectivity. *Water Resources Research*, *37*(8), 2065–2078. https://doi.org/10.1029/2001WR900011

Detournay, E., & Cheng, A. H.-D. (1991). Plane strain analysis of a stationary hydraulic fracture in a poroelastic medium. *International Journal of Solids and Structures*, *27*(13), 1645–1662. https://doi.org/10.1016/0020-7683(91)90067-P

Dorn, C., Linde, N., Le Borgne, T., Bour, O., & Baron, L. (2011). Single-hole GPR reflection imaging of solute transport in a granitic aquifer. *Geophysical Research Letters*, *38*, L08401. https://doi.org/10.1029/2011GL047152

Dreuzy, J. R., Méheust, Y., & Pichot, G. (2012). Influence of fracture scale heterogeneity on the flow properties of three-dimensional discrete fracture networks (DFN). *Journal of Geophysical Research*, *117*, B11207. https://doi.org/10.1029/2012JB009461

Edwards, B., Kraft, T., Cauzzi, C., Kästli, P., & Wiemer, S. (2015). Seismic monitoring and analysis of deep geothermal projects in St Gallen and Basel, Switzerland. *Geophysical Journal International*, *201*(2), 1022–1039. https://doi.org/10.1093/gji/ggv059

Ellsworth, W. L. (2013). Injection-induced earthquakes. *Science*, *341*(6142), 1225942. https://doi.org/10.1126/science.1225942

Evans, K. (2015). Reservoir creation. In S. Hirschberg, S. Wiemer, & P. Burgherr (Eds.), (chap. 3.2, pp. 82–118). Switzerland: vdf Hochschulverlag AG. https://doi.org/10.3218/3655-8

Evans, K. F. (2005). Permeability creation and damage due to massive fluid injections into granite at 3.5 km at Soultz: 2. Critical stress and fracture strength. *Journal of Geophysical Research*, *110*, B04204. https://doi.org/10.1029/2004JB003169

Evans, K. F., Moriya, H., Niitsuma, H., Jones, R. H., Phillips, W. S., Genter, A., Sausse, J., et al. (2005). Microseismicity and permeability enhancement of hydrogeologic structures during massive fluid injections into granite at 3 km depth at the Soultz HDR site. *Geophysical Journal International*, *160*(1), 389–412. https://doi.org/10.1111/j.1365-246X.2004.02474.x

Evans, K. F., Zappone, A., Kraft, T., Deichmann, N., & Moia, F. (2012). A survey of the induced seismic responses to fluid injection in geothermal and CO_2 reservoirs in Europe. *Geothermics*, *41*, 30–54. https://doi.org/10.1016/j.geothermics.2011.08.002

Fairhurst, C. (2003). Stress estimation in rock: A brief history and review. *International Journal of Rock Mechanics and Mining Sciences*, *40*(7-8), 957–973. https://doi.org/10.1016/j.ijrmms.2003.07.002

Ferrari, F., Ziegler, M., Apuani, T., & Loew, S. (2017). Geostatistical analyses of exfoliation and tectonic joint set spacing in alpine granites (Aar Valley, Switzerland). *Bulletin of Engineering Geology and the Environment*, 1–24.

Gao, K., & Harrison, J. P. (2018). Multivariate distribution model for stress variability characterisation. *International Journal of Rock Mechanics and Mining Sciences*, *102*, 144–154. https://doi.org/10.1016/j.ijrmms.2018.01.004

Gaucher, E., Schoenball, M., Heidbach, O., Zang, A., Fokker, P. A., van Wees, J.-D., & Kohl, T. (2015). Induced seismicity in geothermal reservoirs: A review of forecasting approaches. *Renewable and Sustainable Energy Reviews*, *52*, 1473–1490. https://doi.org/10.1016/j.rser.2015.08.026

Gelman, A., Carlin, J. B., Stern, H. S., Dunson, D. B., Vehtari, A., & Rubin, D. B. (2014). *Bayesian data analysis*, (Vol. 2). Boca Raton, FL: CRC press.

Gelman, A., Carlin, J. B., Stern, H. S., & Rubin, D. B. (2004). *Bayesian data analysis*, *Texts in statistical science series*, (). Boca Raton, FL: Chapman & Hall/CRC.

Genter, A., Evans, K., Cuenot, N., Fritsch, D., & Sanjuan, B. (2010). Contribution of the exploration of deep crystalline fractured reservoir of Soultz to the knowledge of enhanced geothermal systems (EGS) Comptes Rendus. *Geoscience*, *342*(7-8), 502–516. https://doi.org/10.1016/j.crte.2010.01.006.

Geyer, C. J. (2011). *Introduction to Markov chain Monte Carlo. Handbook of Markov chain Monte Carlo*. In S. Brooks, et al. (Eds.) (pp. 3–48). Boca Raton, FL: Chapman & Hall/CRC.

Ghassemi, A. (2012). A review of some rock mechanics issues in geothermal reservoir development. *Geotechnical and Geological Engineering*, *30*(3), 647–664. https://doi.org/10.1007/s10706-012-9508-3

Giardini, D. (2009). Geothermal quake risks must be faced. *Nature*, *462*(7275), 848. https://doi.org/10.1038/462848a–849.

Haimson, B. (1968). Hydraulic fracturing in porous and nonporous rock and its potential for determining in situ stresses at great depth, PhD Thesis, University of Minnesota

Häring, M. O., Schanz, U., Ladner, F., & Dyer, B. C. (2008). Characterisation of the Basel 1 enhanced geothermal system. *Geothermics*, *37*(5), 469–495. https://doi.org/10.1016/j.geothermics.2008.06.002

Hickman, S. H., & Davatzes, N. C. (2010). In-situ stress and fracture characterization for planning of an EGS stimulation in the Desert Peak Geothermal Field, Nevada

Illman, W. A., Liu, X., Takeuchi, S., Yeh, T.-C. J., Ando, K., & Saegusa, H. (2009). Hydraulic tomography in fractured granite: Mizunami Underground Research site, Japan. *Water Resources Research*, *45*, W01406. https://doi.org/10.1029/2007WR006715

Jalali, M. (2013). Thermo-hydro-mechanical behavior of conductive fractures using a hybrid finite difference–displacement discontinuity method

Jiménez, S., Mariethoz, G., Brauchler, R., & Bayer, P. (2016). Smart pilot points using reversible-jump Markov-chain Monte Carlo. *Water Resources Research*, *52*, 3966–3983. https://doi.org/10.1002/2015WR017922

Karra, S., O'malley, D., Hyman, J., Viswanathan, H., & Srinivasan, G. (2018). Modeling flow and transport in fracture networks using graphs. *Physical Review E*, *97.3*, 033304.

Lecampion, B., & Lei, T. (2010). Reconstructing the 3D initial stress state over reservoir geo-mechanics model from local measurements and geological priors: A Bayesian approach Schlumberger. *Journal of Modeling, Design and Simulation*, *1*, 100–104.

Lee, J., & Kitanidis, P. (2013). Bayesian inversion with total variation prior for discrete geologic structure identification. *Water Resources Research*, *49*, 7658–7669. https://doi.org/10.1002/2012WR013431

Lei, Q., & Gao, K. (2018). Correlation between fracture network properties and stress variability in geological media. *Geophysical Research Letters*, *45*, 3994–4006. https://doi.org/10.1002/2018GL077548

Lin, W., Yamamoto, K., Ito, H., Masago, H., & Kawamura, Y. (2008). Estimation of minimum principal stress from an extended leak-off test onboard the Chikyu drilling vessel and suggestions for future test procedures. *Scientific Drilling*, *6*, 43–47. https://doi.org/10.5194/sd-6-43-2008

Ljunggren, C., Chang, Y., Janson, T., & Christiansson, R. (2003). An overview of rock stress measurement methods. *International Journal of Rock Mechanics and Mining Sciences*, *40*(7-8), 975–989. https://doi.org/10.1016/j.ijrmms.2003.07.003

Mardia, K. V., Nyirongo, V. B., Walder, A. N., Xu, C., Dowd, P. A., Fowell, R. J., & Kent, J. T. (2007). Markov chain Monte Carlo implementation of rock fracture modelling. *Mathematical Geology*, *39*(4), 355–381. https://doi.org/10.1007/s11004-007-9099-3

Martin, C. D., Read, R. S., & Chandler, N. A. (1990). Does scale influence in situ stress measurements? Some findings at the underground research laboratory, in Scale Effects in Rock Masses. In A. Pinto da Cunda (Ed.), *Proceedings of the First International Workshop on Scale Effects in Rock Masses* (pp. 307–316). Brookfield, Vt.: A. A. Balkema.

Martin, C. D., Read, R. S., & Lang, P. A. (1990). Seven years of in situ stress measurements at the URL An overview. The 31th U.S. Symposium on Rock Mechanics (USRMS), Golden, Colorado, 1990/1/1/

McNamara, D. D., Massiot, C., Lewis, B., & Wallis, I. C. (2015). Heterogeneity of structure and stress in the Rotokawa Geothermal Field, New Zealand. *Journal of Geophysical Research: Solid Earth*, *120*, 1243–1262. https://doi.org/10.1002/2014JB011480

Moeck, I., Bloch, T., Graf, R., Heuberger, S., Kuhn, P., Naef, H., et al. (2015). The St. Gallen project: Development of fault controlled geothermal systems in urban areas. In *Proceedings World Geothermal Congress 2015*. Melbourne, Australia, 19–25 April.

Moein, M., Valley, B., & Ziegler, M. (2016). Preliminary fractal analysis of fracture spacing inferred from an acoustic televiewer log run in the Basel-1 geothermal well (Switzerland). In *Rock mechanics and rock engineering: From the past to the future*, (pp. 1103–1107). Ürgüp, Turkey: ISRM International Symposium - EUROCK 2016, International Society for Rock Mechanics and Rock Engineering.

Mondal, A., Efendiev, Y., Mallick, B., & Datta-Gupta, A. (2010). Bayesian uncertainty quantification for flows in heterogeneous porous media using reversible jump Markov chain Monte Carlo methods. *Advances in Water Resources*, *33*(3), 241–256. https://doi.org/10.1016/j.advwatres.2009.10.010

Moriya, H., Niitsuma, H., & Baria, R. (2003). Multiplet-clustering analysis for estimation of fine detail structures in seismic clouds at Soultz field, France. *Bulletin of the Seismological Society of America*, *93*(4), 1606–1620. https://doi.org/10.1785/0120020072

Pierdominici, S., Mariucci, M. T., & Montone, P. (2011). A study to constrain the geometry of an active fault in southern Italy through borehole breakouts and downhole logs. *Journal of Geodynamics*, *52*(3-4), 279–289. https://doi.org/10.1016/j.jog.2011.02.006

Pollard, D., & Segall, P. (1987). Theoretical displacements and stresses near fractures in rock: with applications to faults, joints, veins, dikes, and solution surfaces. *Fracture Mechanics of Rock*, *277*, 277–349.

Preisig, G., Eberhardt, E., Gischig, V., Roche, V., van der Baan, M., Valley, B., Kaiser, P. K., et al. (2015). Development of connected permeability in massive crystalline rocks through hydraulic fracture propagation and shearing accompanying fluid injection. *Geofluids*, *15*(1-2), 321–337. https://doi.org/10.1111/gfl.12097

Rajabi, M., Tingay, M., King, R., & Heidbach, O. (2017). Present-day stress orientation in the Clarence-Moreton Basin of New South Wales, Australia: A new high density dataset reveals local stress rotations. *Basin Research*, *29*, 622–640. https://doi.org/10.1111/bre.12175

Rutqvist, J. (2015). Fractured rock stress-permeability relationships from in situ data and effects of temperature and chemical-mechanical couplings. *Geofluids*, *15*(1-2), 48–66. https://doi.org/10.1111/gfl.12089

Sahara, D. P., Schoenball, M., Kohl, T., & Müller, B. I. (2014). Impact of fracture networks on borehole breakout heterogeneities in crystalline rock. *International Journal of Rock Mechanics and Mining Sciences*, *71*, 301–309. https://doi.org/10.1016/j.ijrmms.2014.07.001

Salamon, M. (1963). Elastic analysis of displacements and stresses induced by the mining of seam or reef deposits. *Journal of the Southern African Institute of Mining and Metallurgy*, *64*, 128–149.

Schmitt, D. R., Currie, C. A., & Zhang, L. (2012). Crustal stress determination from boreholes and rock cores: Fundamental principles. *Tectonophysics*, *580*, 1–26. https://doi.org/10.1016/j.tecto.2012.08.029

Schoenball, M., & Davatzes, N. C. (2017). Quantifying the heterogeneity of the tectonic stress field using borehole data. *Journal of Geophysical Research: Solid Earth*, *122*, 6737–6756. https://doi.org/10.1002/2017JB014370

Shamir, G., & Zoback, M. D. (1992). Stress orientation profile to 3.5 km depth near the San Andreas fault at Cajon Pass, California. *Journal of Geophysical Research*, *97*(B4), 5059–5080. https://doi.org/10.1029/91JB02959

Sneddon, I. N. (1951). Fourier Transforms (1st ed.). *International Series in Pure and Applied Mathematics* (542 pp.). McGraw-Hill, New York.

Somogyvári, M., Jalali, M., Jimenez Parras, S., & Bayer, P. (2017). Synthetic fracture network characterization with transdimensional inversion. *Water Resources Research*, *53*, 5104–5123. https://doi.org/10.1002/2016WR020293

Stephansson, O., & Zang, A. (2012). ISRM suggested methods for rock stress estimation, part 5: establishing a model for the in situ stress at a given site. *Rock Mechanics and Rock Engineering*, *45*(6), 955–969. https://doi.org/10.1007/s00603-012-0270-x

Tester, J. W., Anderson, B. J., Batchelor, A. S., Blackwell, D. D., DiPippo, R., Drake, E. M., et al. (2006) The Future of geothermal energy; impact of enhanced geothermal systems (EGS) on the United States in the 21st century (Technical report INL/EXT-06-11746). Idaho National Laboratory.

Tezuka, K., & Watanabe, K. (2000). Fracture network modeling of Hijiori hot dry rock reservoir by deterministic and stochastic crack network simulator (D/SC). In *Proceedings World Geothermal Congress 2000* (pp. 3933–3938). International Geothermal Association.

Torabi, A., & Berg, S. S. (2011). Scaling of fault attributes: A review Marine and Petroleum. *Geology*, *28*, 1444–1460.

Tsang, C.-F., Figueiredo, B., & Niemi, A. (2018). Importance of stress effects on inputs to fracture network models used for subsurface flow and transport studies. *International Journal of Rock Mechanics and Mining Sciences*, *101*, 13–17. https://doi.org/10.1016/j.ijrmms.2017.11.012

Valley, B., Dezayes, C., & Genter, A. (2007). Multiscale fracturing in the Soultz-sous-Forêts basement from borehole image analyses. In *Proceedings EHDRA Scientific Conference, 28 & 29 June 2007* (14 pp.). France: Soultz-sous-Forêts.

Valley, B., & Evans, K. (2014). Preliminary assessment of the scaling relationships of in-situ stress orientation variations indicated by wellbore failure data The 2014 ISRM European Rock Mechanics Symposium (EUROCK 2014). In L. R. Alejano, Á. Perucho, C. Olalla, & R. Jiménez (Eds.), *Eurock 2014: Rock Engineering and Rock Mechanics: Structure in and on Rock Masses* (pp. 463–468). Vigo, Spain: CRC Press.

Valley, B., & Evans, K. (2007). Stress state at Soultz-sous-Forêts to 5 km depth from wellbore failure and hydraulic observations. In *Proceedings of the 32nd workshop on geothermal reservoir engineering*. Stanford, CA: Stanford University.

Valley, B., & Evans, K. F. (2009). Stress orientation to 5 km depth in the basement below Basel (Switzerland) from borehole failure analysis. *Swiss Journal of Geosciences*, *102*(3), 467–480. https://doi.org/10.1007/s00015-009-1335-z

Valley, B., & Evans, K. F. (2015). Estimation of the stress magnitude in Basel enhanced geothermal system. In *Proceedings World Geothermal Congress* (12 pp.). Melbourne, Australia.

Valley, B., Jalali, M. R., Ziegler, M., & Evans, K. F. (2014). *Constraining DFN characteristics for deep geothermal projects by considering the effects of fractures on stress variability International Discrete Fracture Network Engineering Conference DFNE 2014*. BC, Canada: Vancouver.

Valley, B. C. (2007). The relation between natural fracturing and stress heterogeneities in deep-seated crystalline rocks at Soultz-sous-Forêts (France). Diss., Naturwissenschaften, Eidgenössische Technische Hochschule ETH Zürich, Nr. 17,385, 2007

Williams-Stroud, S., Kilpatrick, J., Cornette, B., Eisner, L., & Hall, M. (2010). Moving outside of the borehole: Characterizing natural fractures through microseismic monitoring First Break 28

Yale, D. P. (2003). Fault and stress magnitude controls on variations in the orientation of in situ stress. *Geological Society of London, Special Publication*, *209*(1), 55–64. https://doi.org/10.1144/GSL.SP.2003.209.01.06

Zha, Y., Yeh, T.-C. J., Illman, W. A., Tanaka, T., Bruines, P., Onoe, H., & Saegusa, H. (2015). What does hydraulic tomography tell us about fractured geological media? A field study and synthetic experiments. *Journal of Hydrology*, *531*, 17–30.

Ziegler, M., Loew, S., & Bahat, D. (2014). Growth of exfoliation joints and near-surface stress orientations inferred from fractographic markings observed in the upper Aar valley (Swiss Alps). *Tectonophysics*, *626*, 1–20. https://doi.org/10.1016/j.tecto.2014.03.017

Ziegler, M., Loew, S., & Moore, J. R. (2013). Distribution and inferred age of exfoliation joints in the Aar Granite of the central Swiss Alps and relationship to Quaternary landscape evolution. *Geomorphology*, *201*, 344–362. https://doi.org/10.1016/j.geomorph.2013.07.010

Ziegler, M., Valley, B., & Evans, K. F. (2015). *Characterisation of natural fractures and fracture zones of the Basel EGS reservoir inferred from geophysical logging of the Basel-1 well*. Paper presented at World Geothermal Congress Melbourne, Australia, 19–25 April.

Zoback, M. D. (2010). *Reservoir Geomechanics*. Cambridge, UK: Cambridge University Press.

Zoback, M. D., Barton, C. A., Brudy, M., Castillo, D. A., Finkbeiner, T., Grollimund, B. R., Moos, D. B., et al. (2003). Determination of stress orientation and magnitude in deep wells. *International Journal of Rock Mechanics and Mining Sciences*, *40*(7-8), 1049–1076. https://doi.org/10.1016/j.ijrmms.2003.07.001